Journal of Geophysical Research: Biogeosciences

Supporting Information for

Systematic assessment of retrieval methods for canopy far-red solar-induced chlorophyll fluorescence (SIF) using automated high-frequency field spectroscopy

Christine Y. Chang[1,*], Luis Guanter[2], Christian Frankenberg[3,4], Philipp Köhler[3], Lianhong Gu[5], Troy Magney[6], Katja Grossmann[7], Ying Sun[1,*]

[1] School of Integrative Plant Science, Soil and Crop Sciences Section, Cornell University, Ithaca, NY, USA
[2] Centro de Tecnologías Físicas, Universitat Politècnica de València, Camí de Vera s/n, 46022 València, Spain
[3] Division of Geological and Planetary Sciences, California Institute of Technology, Pasadena, CA, USA
[4] Jet Propulsion Laboratory, California Institute of Technology, Pasadena, CA, US
[5] Environmental Sciences Division and Climate Change Institute, Oak Ridge National Laboratory, Oak Ridge, TN, USA
[6] Department of Plant Sciences, University of California Davis, Davis, CA, USA
[7] Institute of Environmental Physics, University of Heidelberg, Heidelberg, Germany

[*]Corresponding authors: Christine Y. Chang (cyc54@cornell.edu) and Ying Sun (ys776@cornell.edu)

Contents of this file

Figures S1 to S9
Tables S1 to S2

Introduction

These supplementary materials include supporting figures and tables. A detailed description of the methods and materials used in the figures below are found in the main text.

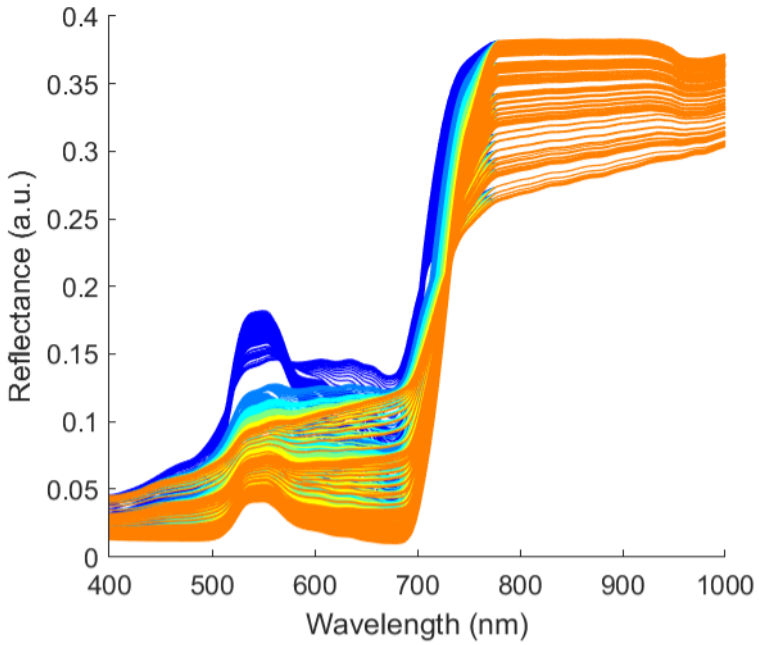

Figure S1. Spectral shapes of reflectance ρ generated by combinations of leaf area index (LAI) and total chlorophyll content (Chl) using SCOPE. Visible and near-infrared reflectance simulated by SCOPE (400-1000nm). Colors represent different levels of Chl (cooler colors indicate lower Chl, warmer colors indicate higher Chl). Line weights represent different levels of LAI (thicker lines indicate higher LAI).

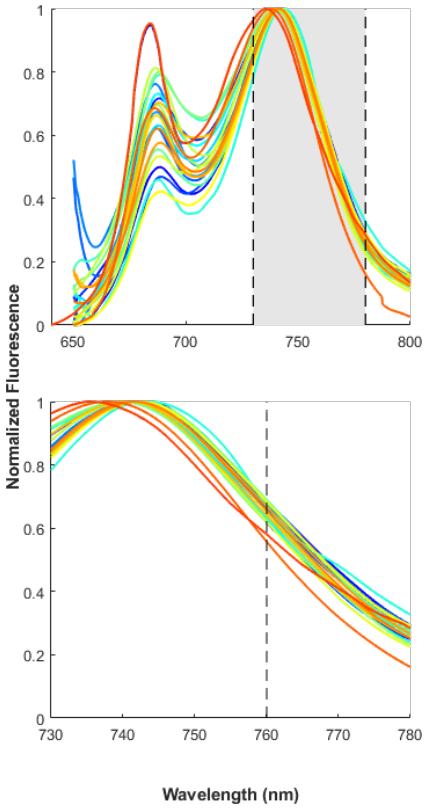

Figure S2. SIF spectra (h_F) used for SIF simulation. Values are normalized so the peak value = 1. QE Pro range used in this study is highlighted in gray.

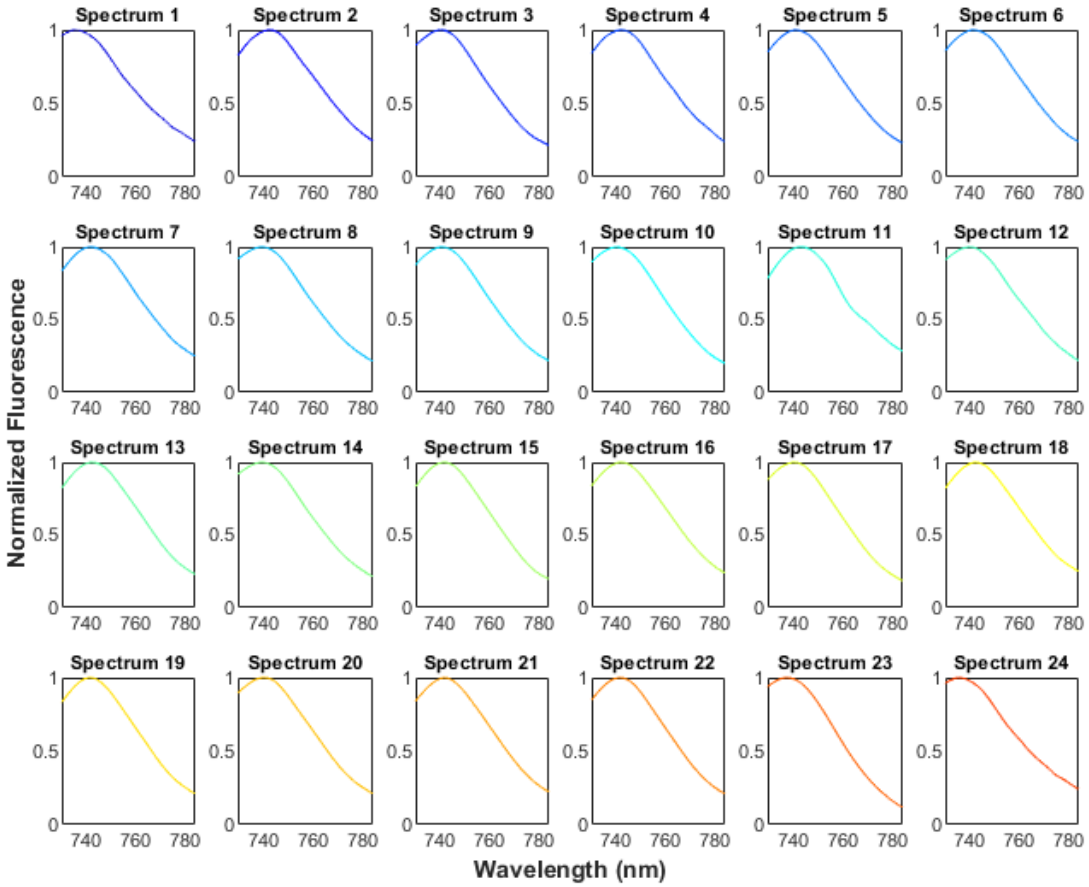

Figure S3. Individual prescribed shapes of 24 fluorescence spectra used for SIF simulation. Fluorescence spectra are scaled so the peak maximum = 1.

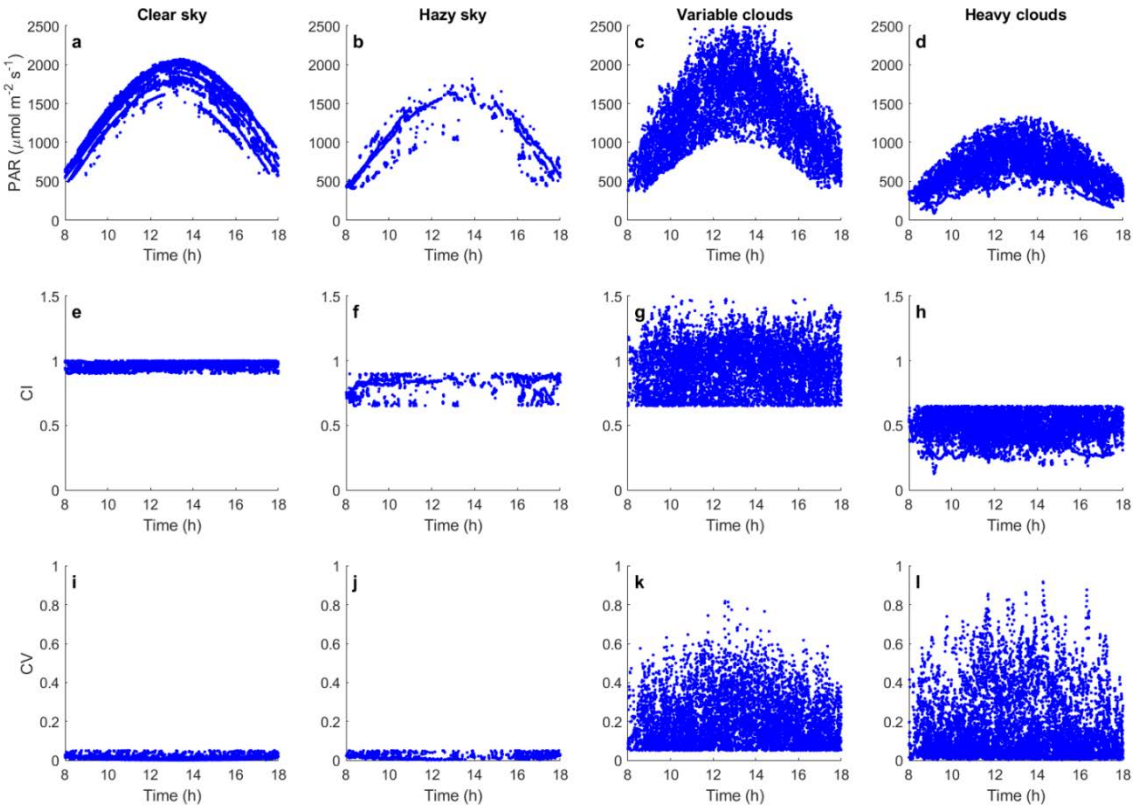

Figure S4. Conditions used to categorize different sky conditions. Top row (a-d): PAR recorded under each condition across the growing season; middle row (e-h): clearness index (CI) of all measurements under each sky condition; bottom row (i-l): coefficient of variation (CV) of all measurements under each sky condition.

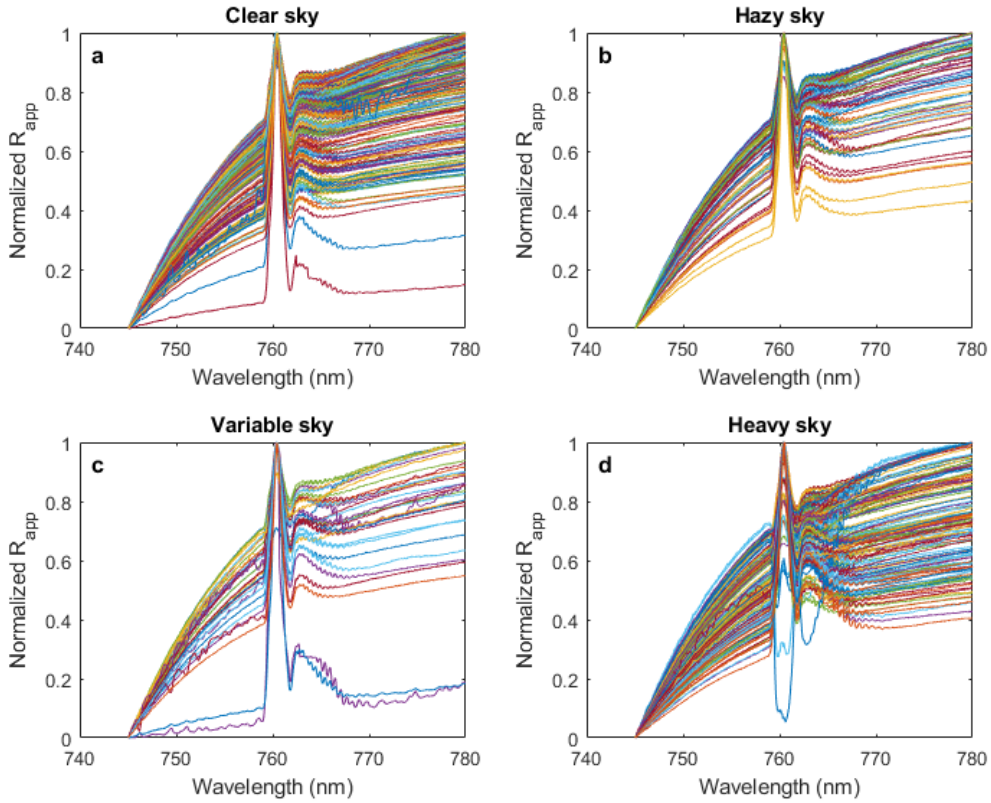

Figure S5. PhotoSpec spectra prior to baseline screening.

Here, the apparent reflectance (Rapp) from 745-780 nm is normalized to 0-1 range as (Rapp - min(Rapp)) / (max(Rapp) - min(Rapp)). Each line represents the mean of 13 apparent reflectance spectra recorded across -78° to -87° VZA across two VAZ, classified under the corresponding sky condition using the criteria described in Section 2.4. Spectra with clear anomalous baseline features (large ridges) are visible in panels a,c,d.

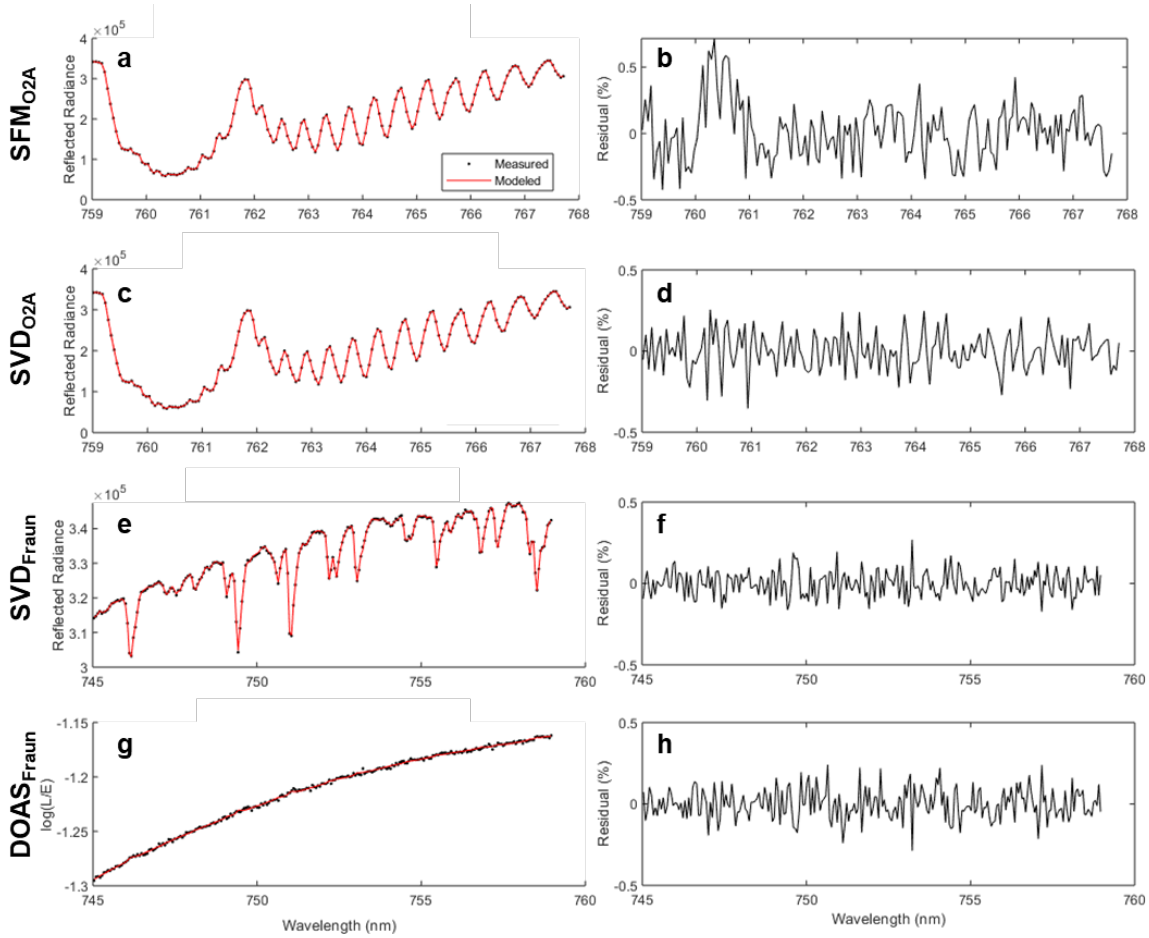

Figure S6. Example model fit and residuals for SIF retrievals from field measurements shown in Figure 1. Left column (a,c,e,g): measured and modeled *L* spectra or logarithm of apparent reflectance; right column (b,d,f,h): fitting residuals. SIF is retrieved using (a,b) SFMO2A with fitting window 759-767.76 nm; (c,d) SVD_{O2A} with fitting window 759-767.76 nm, trained using all *E* spectra measured during each day; (e,f) SVD_{Fraun}, trained using all *E* spectra measured during each day; (e) $DOAS_{Fraun}$. Examples are taken from a midday measurement on clear day (DOY 200).

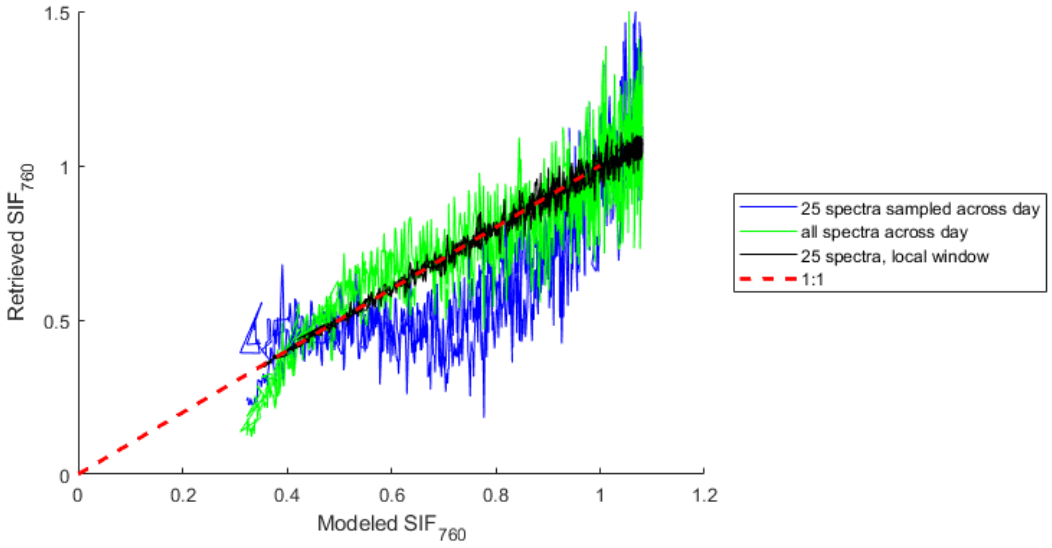

Figure S7. Diurnal distortion of SIF retrieved by SVD trained with and without temporally constrained sample set. Here, synthetic *L* is generated from one clear day (DOY 200) for testing retrieval accuracy. SIF is retrieved using SVD trained using either 25 *E* spectra randomly sampled across the day (blue), all *E* spectra sampled across the day (green), or 25 *E* spectra sampled from a temporally constrained window.

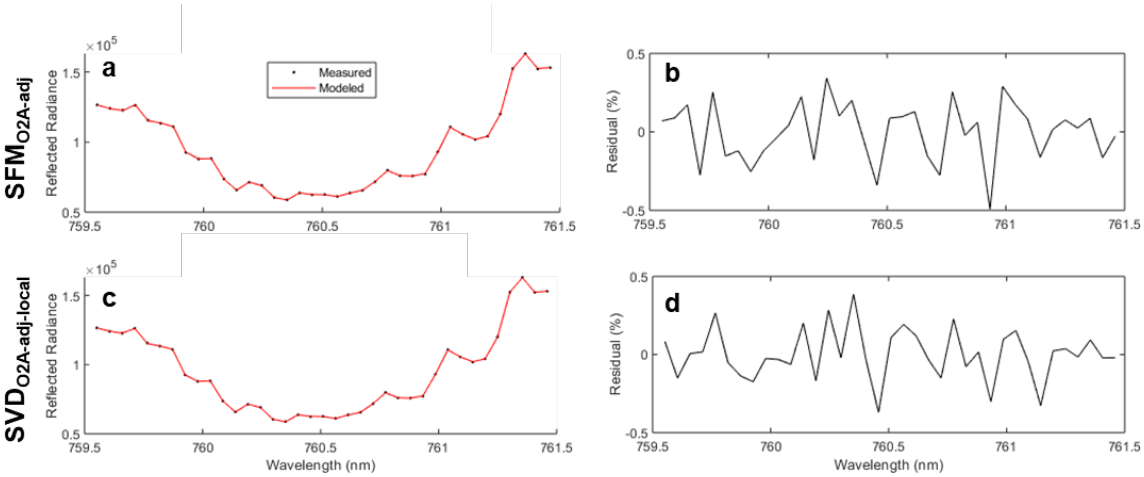

Figure S8. Example model fit and residuals for SIF retrievals from field measurements shown in Figure 5. Left column (a,c): measured and modeled *L* spectra; right column (b,d): fitting residuals. SIF is retrieved using (a,b) SFM_{O2A} with fitting window 759.5-761.5 nm; (c,d) SVD_{O2A} with fitting window 759.5-761.5 nm, trained using a moving window of five local *E* spectra. Examples are taken from a midday measurement on clear day (DOY 200).

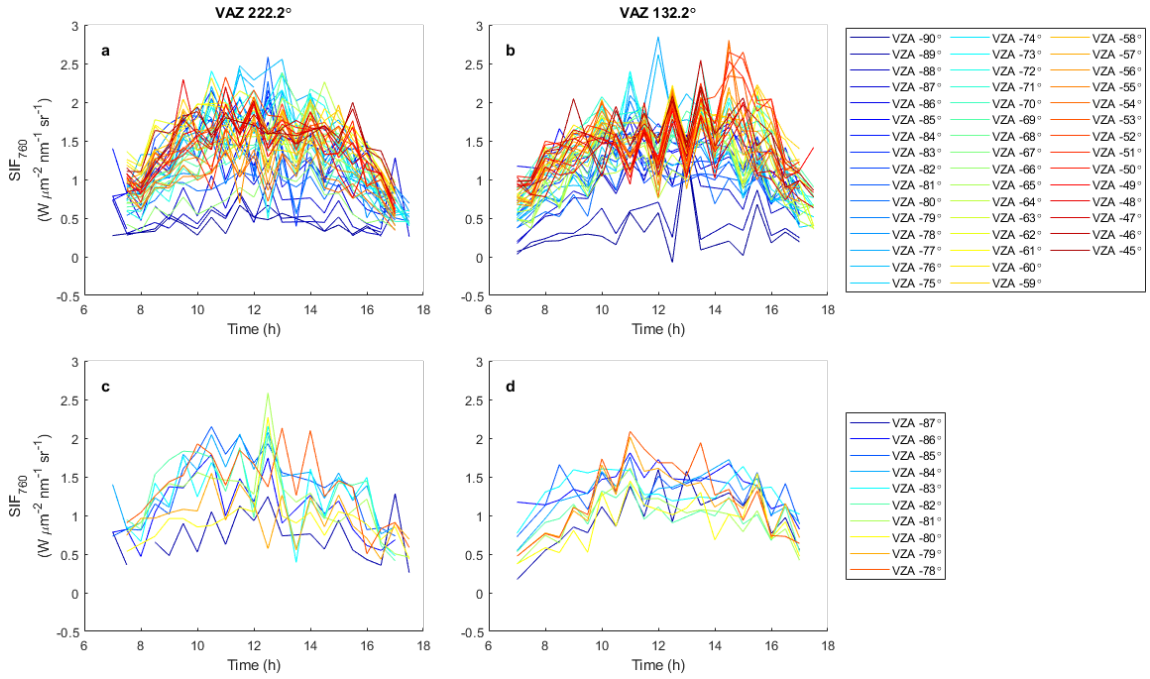

Figure S9. Angle effects on SIF diurnal pattern retrieved using different combinations of viewing zenith and viewing azimuth angles from a hemispherical-conical system.

(a,b) SIF retrieved for each viewing zenith angle recorded at each viewing azimuth angle under clear sky conditions. (c,d) Same as (a,b) but only showing the viewing zenith angles used in the present study for visual clarity. (a,c) Morning hysteresis was observed when non-nadir spectra were recorded from southwest-facing direction; (b,d) afternoon hysteresis was observed when non-nadir spectra were recorded from southeast-facing direction. Here only SIF retrieved using $SFM_{O2A\text{-}adj}$ is used for illustration purposes; a similar divergence in diurnal SIF patterns between VAZ is observed with other retrieval methods.

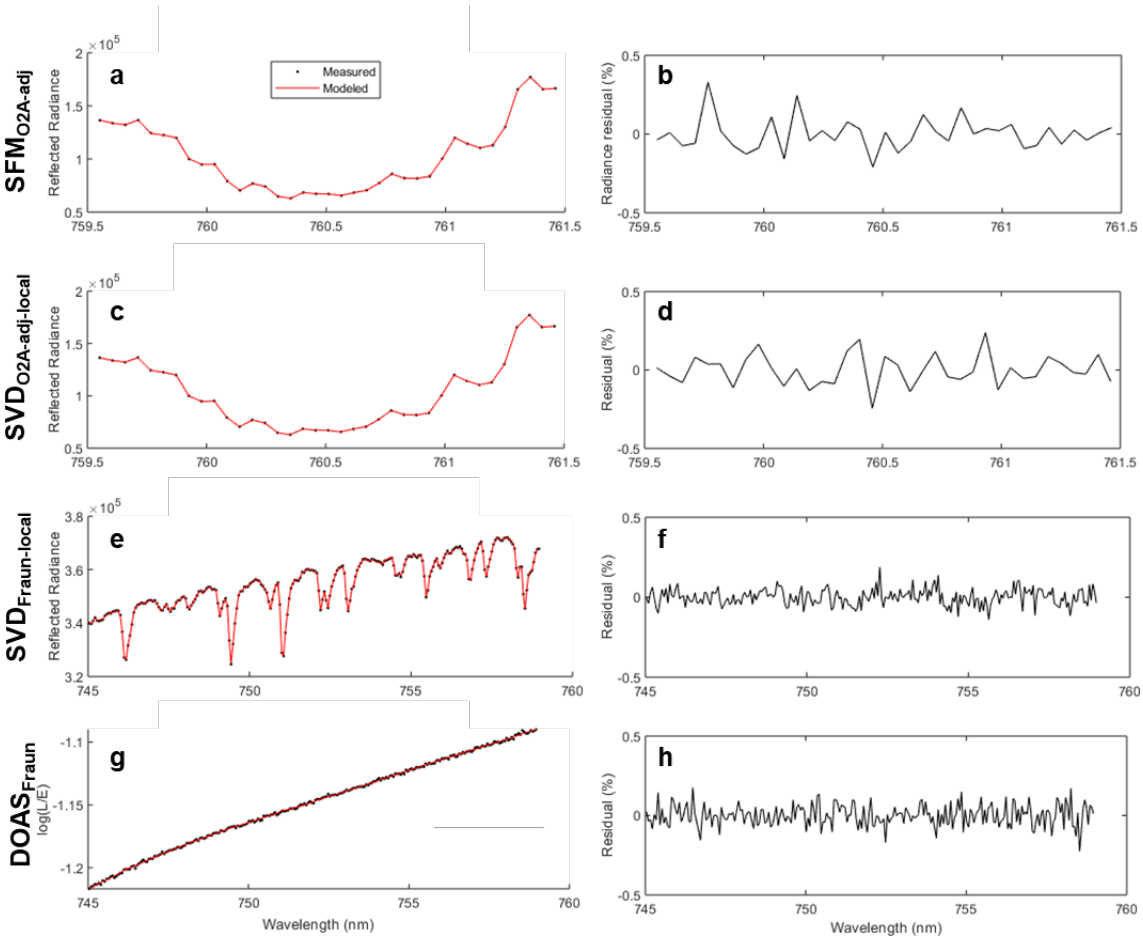

Figure S10. Example model fit and residuals for synthetic SIF retrievals shown in Figure 8. Left column (a,c): measured and modeled *L* spectra; right column (b,d): fitting residuals. SIF is retrieved using (a,b) SFM_{O2A} with fitting window 759.5-761.5 nm; (c,d) SVD_{O2A} with fitting window 759.5-761.5 nm, trained using a moving window of five local *E* spectra; (e,f) SVD_{Fraun} with fitting window 745-759 nm, trained using a moving window of five local *E* spectra; (g,h) $DOAS_{Fraun}$.

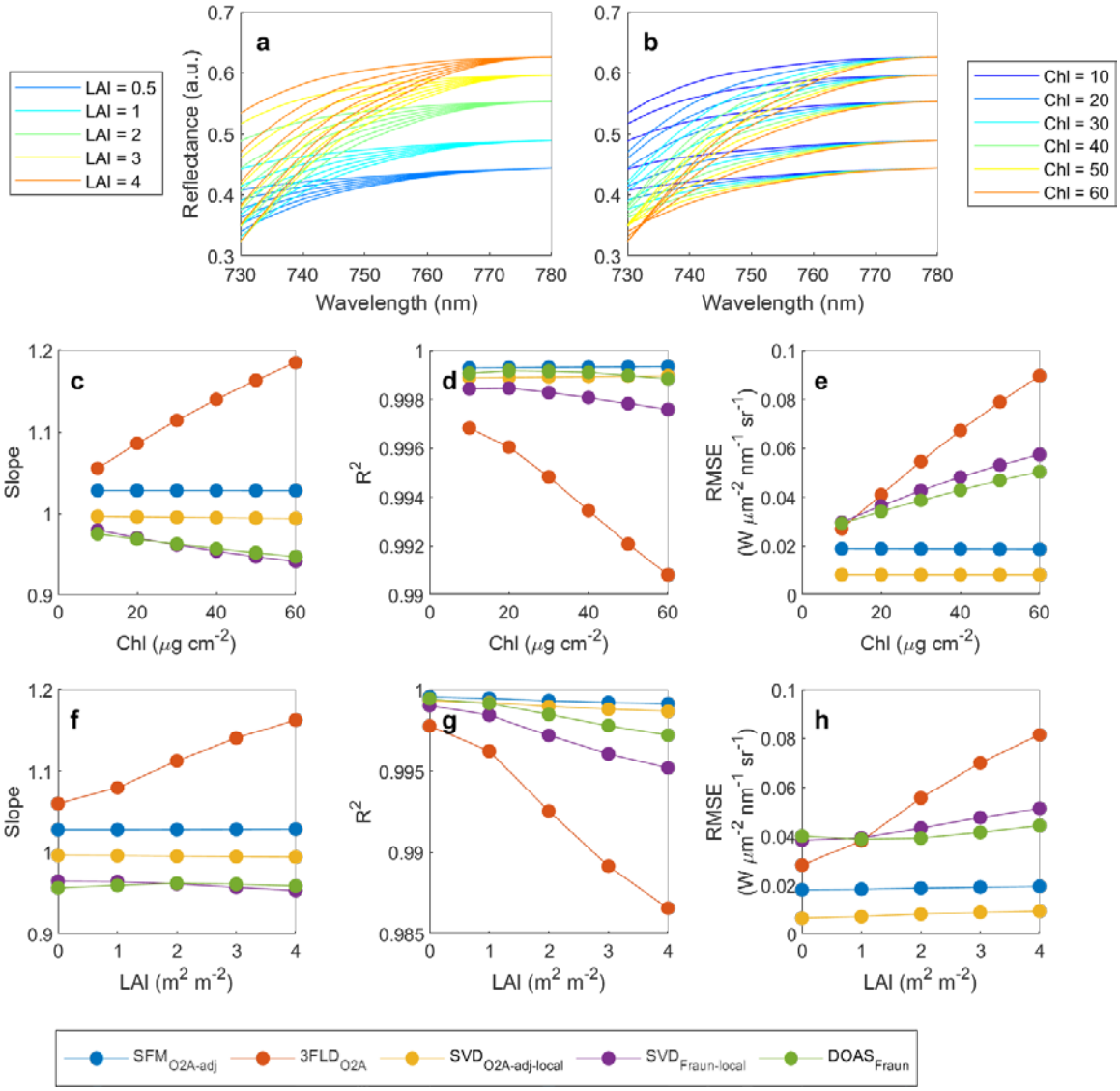

Figure S11. Sensitivity of SIF retrieval accuracy to the assumed spectral shape of reflectance caused by Chl and LAI variation; similar to Figure 11 but generated using PROSAIL reflectance. (a, b) ρ simulated by PROSAIL using different levels of Chl and LAI. (c-h) Half-hourly mean SIF retrieved using $SFM_{O2A\text{-}adj}$, $3FLD_{O2A}$, $SVD_{O2A\text{-}adj\text{-}local}$, $SVD_{Fraun\text{-}local}$ or $DOAS_{Fraun}$ from *L* spectra simulated using (c-e) different levels of Chl with LAI = 4 m^2 m^{-2} or (f-h) different levels of LAI with 60 µg cm^{-2} Chl. (c,f) Slope, (d,g) R^2 or (e,h) RMSE is calculated between half-hourly means of retrieved and simulated SIF_{760}. For this test, *L* is generated using one day of clear sky measurements obtained during the peak growing season (DOY 200).

Table S1. Height and LAI measured at field site during 2018 growing season.

Day of Year	Height (cm)	LAI (m^2 m^{-2})
192	108	1.36
197	127	1.52
200	140	2.07
207	173	2.39
211	183	3.35
227	186	3.42
241	186	3.95
260	186	1.85
267	186	1.99

Table S2. Customized input parameters for SCOPE model. Climate variables were recorded at the field site over the growing season. Pigment content, thickness parameters and leaf angle distribution were set using typical values (Verrelst et al. 2015). SZA and relative azimuth angle were calculated based on latitude, longitude, time of day and day of year. For Experiment 1, LAI and canopy height were measured (see Table S1).

Parameter	Description	Units	Experiment 1	Experiment 2	Experiment 3
Chl	Chlorophyll a+b concentration	μg cm^{-2}	60	[10, 20, 30, 40, 50, 60]	60
Car	Carotenoid concentration	μg cm^{-2}	15	25% of Cab	15
C_{dm}	Dry matter content	g cm^{-2}	0.012	0.012	0.012
C_w	Leaf water equivalent layer	cm	0.009	0.009	0.009
C_s	Senescent material fraction		0	0	0
C_{ant}	Anthocyanins	μg cm^{-2}	0	0	0
N	Leaf thickness parameter		1.4	1.4	1.4
rho_thermal	broadband thermal reflectance		0.01	0.01	0.01
tau_thermal	broadband thermal transmittance		0.01	0.01	0.01
LAI	Leaf Area Index	m^2 m^{-2}	1.42-3.954	[0.5, 1, 2, 3, 4]	4
hc	Vegetation height	m	1.2-1.862	2	2
LIDFa	Leaf inclination distribution		-0.35	-0.35	-0.35
LIDFb	Leaf inclination distribution		-0.15	-0.15	-0.15
leafwidth	leaf width	m	0.1	0.1	0.1
z	measurement height of meteorological data	m	4	4	4
Rin	broadband incoming shortwave radiation (0.4-2.5 μm)	W m^{-2}	0-1030	0-1030	0-1030

Rli	broadband incoming longwave radiation	W m^{-2}	279-448	279-448	279-448
Ta	air temperature	C	9.4-37.2	9.4-37.2	9.4-37.2
ea	vapor pressure	hPa	0-35.6	0-35.6	0-35.6
tto	Viewing zenith angle	degrees	0	0	0
sza	Solar zenith angle	degrees	32.89 – 89.93	32.89 – 89.93	32.89 – 89.93
raa	Relative azimuth angle	degrees	76.00 – 282.68	76.00 – 282.68	76.00 – 282.68